Local signaling with molecular diffusion as a decoder of Ca^{2+} signals in synaptic plasticity

Honda Naoki, Yuichi Sakumura and Shin Ishii*

Graduate School of Information Science, Nara Institute of Science and Technology, Takayama, Ikoma, Nara, Japan
* Corresponding author. Graduate School of Information Science, Nara Institute of Science and Technology, 8916-5 Takayama, Ikoma, Nara 630-0192, Japan.
Tel.: + 81 743 72 5984; Fax: + 81 743 72 5989; E-mail: ishii@is.naist.jp

Synaptic plasticity is induced by the influx of calcium ions (Ca^{2+}) through N-methyl-D-aspartate receptors (NMDARs), and the direction and strength of the response depend on the frequency of the synaptic inputs. Recent studies have shown that the direction of synaptic plasticity is also governed by two distinct NMDAR subtypes (NR1/NR2A, NR1/NR2B). How are the different types of regulation (frequency-dependent and receptor-specific) processed simultaneously? To clarify the molecular basis of this dual dependence of synaptic plasticity, we have developed a mathematical model of spatial Ca^{2+} signaling in a dendritic spine. Our simulations revealed that calmodulin (CaM) activation in the vicinity of NMDARs is strongly affected by the diffusion coefficient of CaM itself, and that this 'local CaM diffusion system' works as a dual decoder of both the frequency of Ca^{2+} influxes and their postsynaptic current shapes, generated by two NMDAR subtypes, implying that spatial factors may underlie the complicated regulation scheme of synaptic plasticity.
Molecular Systems Biology 13 December 2005; doi:10.1038/msb4100035
Subject Categories: simulation & data analysis; neuroscience
Keywords: local signaling; molecular diffusion; NMDA receptor subtypes; mathematical model

Introduction

Ca^{2+} ions play a role in triggering signal transduction pathways that regulate a variety of neurobiological processes including synaptic plasticity, one of the major mechanisms underlying learning and memory. In a neuron, Ca^{2+} signaling is spatiotemporally regulated both globally, within a cellular compartment such as a dendritic spine, and locally at the site of Ca^{2+} entry. Thus, the differences between local and global Ca^{2+} signaling must be elucidated in order to fully understand the spatial regulation of signal transduction cascades.

The frequency of synaptic inputs, and hence the frequency of Ca^{2+} influxes caused by N-methyl-D-aspartate receptor (NMDAR) activation, is thought to dictate the direction and strength of synaptic plasticity (Dudek and Bear, 1992; Markram *et al*, 1997; Johnston *et al*, 2003). It was reported recently, however, that the direction of synaptic plasticity is also governed by NR2A- and NR2B-containing NMDAR subtypes; the induction of long-term potentiation (LTP) is blocked by antagonists of NR2A but not of NR2B, whereas the induction of long-term depression (LTD) is blocked by antagonists of NR2B but not of NR2A (Liu *et al*, 2004a; Massey *et al*, 2004). This implies a controversial 'receptor-specific regulation' of synaptic plasticity (Bliss and Schoepfer, 2004; Rusakov *et al*, 2004; Wong *et al*, 2004). How the distinct characteristics of synaptic plasticity (i.e., frequency-dependent and receptor-specific regulation) are realized simultaneously has yet to be elucidated.

With respect to global Ca^{2+} signaling within an entire dendritic spine, there is a potential problem with receptor-specific regulation. Because Ca^{2+} diffusion is very rapid, and the volume of a dendritic spine is relatively small ($<1\,\mu m^3$), the Ca^{2+} concentration should, in effect, become instantaneously uniform within a spine. If so, downstream signals originating from different Ca^{2+} sources are likely to become entangled. This problem could be avoided if the downstream signaling works specifically in the so-called Ca^{2+} nano-domain, an area with a relatively high Ca^{2+} concentration localized near Ca^{2+} channels (Augustine *et al*, 2003).

Studies in hippocampal neurons have indicated that molecular regulation in local Ca^{2+} signaling is associated with changes in synaptic weight. An electrophysiological study using two different exogenous Ca^{2+} buffers, BAPTA and EGTA, provided circumstantial evidence of local Ca^{2+} signaling around NMDARs during the induction of LTP (Hoffman *et al*, 2002). Moreover, a Ca^{2+} imaging experiment has shown that L-type voltage-sensitive Ca^{2+} channels do not contribute measurably to increasing Ca^{2+} levels in spines, but instead to activating calcium/calmodulin (CaM)-dependent kinase II (CaMKII), suggesting the existence of local Ca^{2+} signaling (Yasuda *et al*, 2003). Immunohistochemical studies have shown that plasticity-related molecules, such as CaMKII and protein phosphatase 1 (PP1), are localized at the postsynaptic densities (PSDs) just below synaptic membranes (Sheng and Lee, 2000; Winder and Sweatt, 2001; Blackstone and Sheng,

2002; Lisman *et al*, 2002; Petersen *et al*, 2003). The significance of local Ca^{2+} signaling can also be predicted computationally in simulation studies of Ca^{2+} signaling. When the signaling pathway was modeled as a uniform system, the computed level of CaM activation was low and insufficient to upregulate CaMKII (Bhalla, 2002a, b), probably due to the lack of spatially localized reactions. Despite this evidence of local Ca^{2+} signaling, its role in the regulation of synaptic plasticity has not yet been clarified.

The diffusion of Ca^{2+} is so rapid that it is probably difficult to regulate local Ca^{2+} signaling in small components such as dendritic spines. In this study, we focus on local signaling mediated by CaM instead of Ca^{2+} itself, because CaM diffuses relatively slowly, and hence allow for flexible control on the signaling. CaM, a Ca^{2+} effector protein, is a primary transducer that mediates the Ca^{2+}-regulated inductions of synaptic plasticity (Xia and Storm, 2005).

The effects of molecular diffusion must be considered as local regulation, because molecular diffusion should be physically and chemically impeded if proteins accumulate to a high level in a local space. In fact, the abundance of actin filaments and PSD-95 (a scaffolding protein) under synaptic membranes is a remarkable aspect of dendritic spines (Kennedy, 2000; Matus, 2000). Furthermore, the *in vivo* suppression of molecular diffusion has been reported in neurons and smooth muscle cells (Popov and Poo, 1992; Luby-Phelps *et al*, 1995); this impedance should contribute to the local molecular regulation of synaptic plasticity.

To examine the contributions of local reactions in the Ca^{2+} nano-domain and the impeded diffusion of CaM to the regulation of synaptic plasticity, we have constructed a mathematical model of spatial Ca^{2+} signaling in a dendritic spine, in which Ca^{2+} flows into the cytoplasm and interacts with diffusing CaM. To clarify the molecular basis of the frequency-dependent and receptor-specific regulation of synaptic plasticity, in particular, we have examined the response of local Ca^{2+} signaling while taking into account the frequency and postsynaptic current shapes of Ca^{2+} influxes

generated by two NMDAR subtypes (Erreger *et al*, 2005). First, we show that local Ca^{2+} signaling is regulated in a different manner from global signaling. Second, we shed light on a significant dependence of local CaM dynamics on CaM diffusion, suggesting that to achieve a sufficient level of local CaM activation, the system requires a moderate CaM diffusion coefficient. Third, we demonstrate that as long as CaM is able to diffuse, local Ca^{2+} signaling can process different features of synaptic inputs: the frequency and current shapes of Ca^{2+} influxes. Moderate CaM diffusion enables local Ca^{2+} signaling to act as a 'dual decoder' to translate these input features into the correlated level of CaM activity. We also show that these local dynamics are highly robust to various Ca^{2+}-regulating factors, such as the buffering system and excretion by Ca^{2+} pumps, and hence that the decoding properties are preserved under any conditions. These findings suggest that a 'local CaM diffusion system' functions as the molecular basis of the complicated regulation scheme of synaptic plasticity.

Results

To simulate local dynamics of Ca^{2+} signaling, we constructed a model of spatial Ca^{2+} signaling in a dendritic spine (1 μm^3), which included Ca^{2+} influx through NMDARs, Ca^{2+} uptake by pumps, leakage through the membrane, buffering by Ca^{2+}-binding proteins, and CaM activation (Figure 1A; for details, see Materials and methods and Supplementary Figure 1). To pay attention to the locality of Ca^{2+} signaling, we assumed radial diffusion from a Ca^{2+} source consisting of a cluster of NMDARs.

The difference between local and global Ca^{2+} signaling

To examine the characteristic difference between local and global Ca^{2+} signaling, we first investigated the spatiotemporal details of Ca^{2+} and CaM responding to Ca^{2+} influxes injected through NMDARs. When Ca^{2+} influxes were applied to the
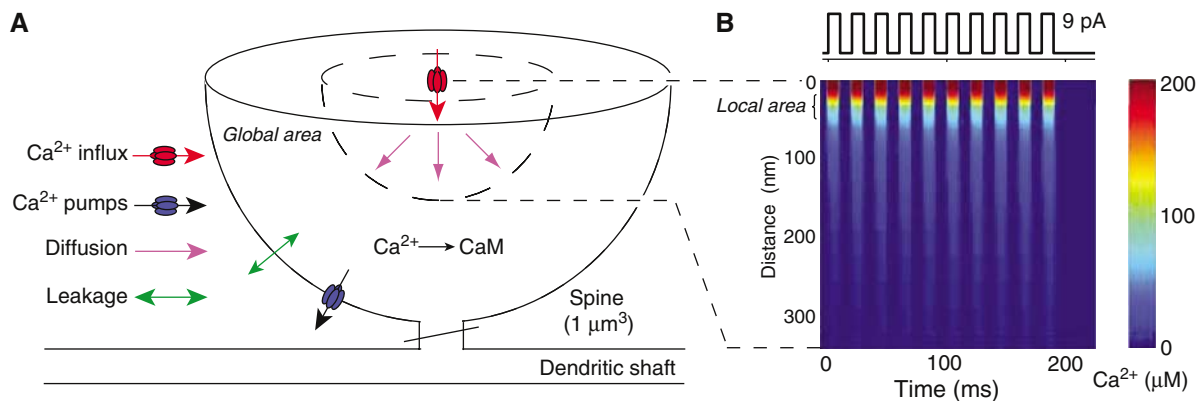

Figure 1 A scheme of a model spine and a local Ca^{2+} profile. (**A**) The model spine is composed of hemispherical elements and has a volume of 1 μm^3. Ca^{2+} ions were injected through NMDARs as a point source located at the center of the spine (red arrow). Diffusing molecules were assumed to diffuse radially from the NMDARs. Ca^{2+} influx, Ca^{2+} uptake by pumps, leakage from the membrane, and buffering by Ca^{2+}-binding proteins were all incorporated into the model. To compare local and global signaling, we focused on the concentrations of Ca^{2+} and CaM in the local and global areas as indicators of the degree of signaling activity at the PSD and in the whole spine, respectively. (**B**) The spatiotemporal Ca^{2+} profile when a sequence of 10 Ca^{2+} influxes was injected at 50 Hz (upper panel) into the model. Each injected current was biologically realistic (amplitude=9 pA, Ca^{2+} fraction=11%, period=10 ms) (Pina-Crespo and Gibb, 2002; Nimchinsky *et al*, 2004). The horizontal axis denotes the elapsed time from the onset of current injection, and the vertical axis denotes the distance from the site of the NMDARs (lower panel).

model spine, a high Ca^{2+} concentration ($>90\,\mu M$) was localized at the Ca^{2+} nano-domain, which is within 50 nm of the influx source ($\approx$ scale of PSDs) (Figure 1B), and its transient time course formed rectangular shapes (Figure 2A, upper panel), reflecting the shapes of the influx time course (Figure 1B, upper panel) (Supplementary Figure 2 shows the case when triangular-shaped currents were applied). Such transient responses of Ca^{2+} in the local area are considered to occur owing to the rapid formation of a Ca^{2+} steady gradient resulting from fast Ca^{2+} diffusion. In contrast to these local Ca^{2+} dynamics, the global Ca^{2+} response was rather slow and cumulative (Figure 2A, lower panel). The cumulative effect of Ca^{2+} depended on the distance from the NMDARs (Figure 2B), as has been suggested by a modeling study of a presynaptic system for the facilitation of vesicle release (Tang *et al*, 2000).

Responding to such Ca^{2+} profiles, CaM was highly activated in the local area, but only weakly activated in the global area (Figure 2C). This high CaM activity in the local area was sufficient to upregulate CaMKII, a CaM effector protein (Supplementary Figure 3). A particularly important aspect of local CaM activation is the accumulation of input stimuli, which is not realized by the local Ca^{2+} concentration. The slower diffusion of CaM than of Ca^{2+} (Figure 2D) induces the accumulation of activated CaM in the local area. In contrast, the obtained global CaM activity was small, less than $0.75\,\mu M$, which was insufficient to upregulate CaMKII (Supplementary Figure 3). This activation was due to diffusion of activated

CaM from the local area, and actually CaM was not activated in the global area when the CaM diffusion was blocked (Supplementary Figure 4). These observations suggest that the regulation of Ca^{2+} signaling should be treated as a spatial system, rather than as a uniform system, which ignores spatial factors, even in a tiny spine.

The behavior of simulated global Ca^{2+} is consistent with biological data. In our simulation, peak concentration was around $1\,\mu M$ and decay time constant was around 23.5 ms (Figure 2A, lower panel). Comparable values were measured by Ca^{2+} imaging studies in dendritic spines (Murthy *et al*, 2000; Holthoff *et al*, 2002; Sabatini *et al*, 2002) (see the comparison of Ca^{2+} decay behavior with experimental data in Supplementary Figure 5). If a Ca^{2+} indicator (Fluo-4, $200\,\mu M$) was added to the model spine in a simulation experiment, peak Ca^{2+} decreased and the decay of global Ca^{2+} concentration became slower (Supplementary Figure 6). To show the adequacy of the model behaviors from a different perspective, we reproduced the experimentally observed effects of exogenous Ca^{2+} buffers, BAPTA and EGTA, on local and global Ca^{2+} signaling (Supplementary Figure 7) (Hoffman *et al*, 2002). Moreover, we checked the robustness of local and global Ca^{2+} signaling against variation in buffering systems, excretion by Ca^{2+} pumps, and spine morphology such as size and geometry. To summarize the results, global Ca^{2+} signaling was sensitive to most of those factors, but local Ca^{2+} signaling was highly robust (Supplementary Figures 8–12).
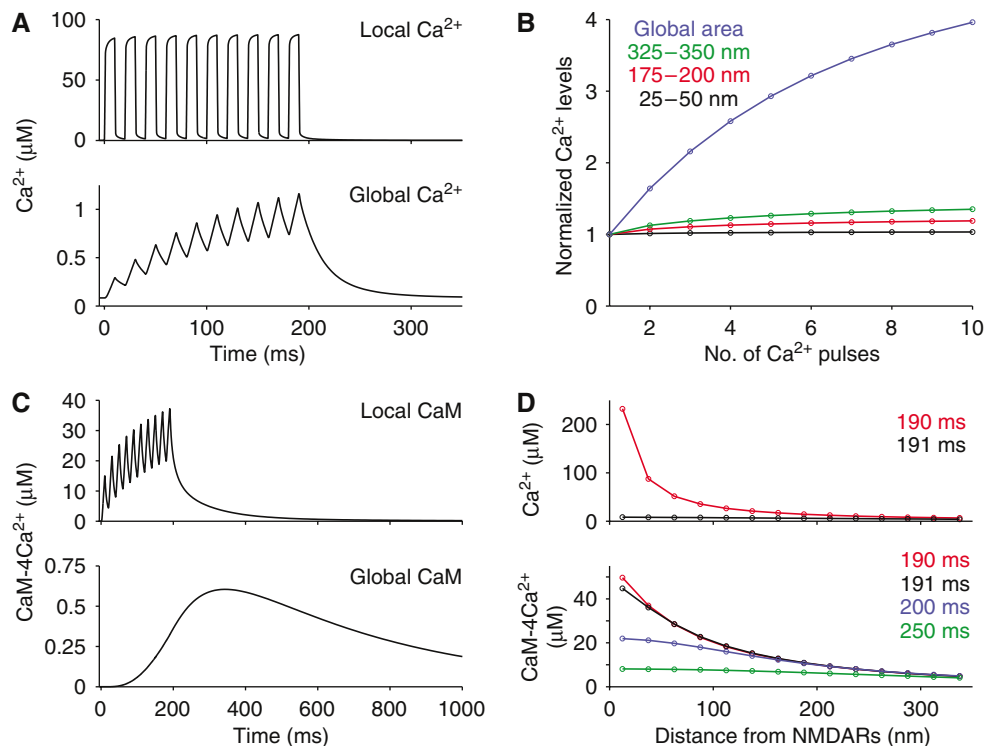
Figure 2 The details of local and global Ca^{2+} signaling. (**A**) The time courses of Ca^{2+} in the local area (25–50 nm away from the NMDARs, upper panel) and in the global area (>350 nm from the NMDARs, lower panel). These curves were extracted from Figure 1B. (**B**) Accumulation effect of Ca^{2+} response, dependent on the distance from NMDARs. Peak Ca^{2+} responses are plotted against the number of input pulses in a burst stimulus (10 pulses) so that each Ca^{2+} peak value at the onset is normalized at 1. (**C**) The time courses of CaM activation in the local (upper panel) and global (lower panel) areas, induced by Ca^{2+} influxes. (**D**) Temporal changes of Ca^{2+} (upper panel) and CaM (lower panel) activities are plotted against the distance from NMDARs. Red, black, blue, and green lines indicate the time of 0, 1, 10, and 60 ms, respectively, elapsed after Ca^{2+} stimulation was finished at 190 ms.

The effects of molecular diffusion on local Ca²⁺ signaling

Local diffusion of CaM may be impeded not only chemically by interaction with CaM effectors, but also physically by the cytoskeleton and scaffolding proteins, because PSDs in dendritic spines contain an abundance of proteins. Indeed, it was found that the diffusion coefficient of receptors moving two-dimensionally on the plasma membrane decreases exponentially as scaffolding proteins accumulate (Nakada *et al*, 2003). To examine the effects of this restricted molecular diffusion on local Ca²⁺ signaling, we investigated CaM activation in the Ca²⁺ nano-domain using various diffusion coefficients for CaM. CaM activation resulting from the high Ca²⁺ level in the local area depended strongly on the diffusion coefficient of CaM (Figure 3B). When the CaM diffusion coefficient estimated *in vitro* (Yang *et al*, 2001) was used, CaM activity was close to zero, as observed in previous simulation studies based on a uniform system (Bhalla, 2002a, b), whereas nondiffusible CaM resulted in CaM activation that exceeded the level required for 100% CaMKII autophosphorylation (Figure 3A and B and Supplementary Figure 3). When the diffusion coefficient of CaM was set to the value observed *in vivo* (Luby-Phelps *et al*, 1995), the level of CaM activation in the local area lay within the controllable range for CaMKII autophosphorylation (green line in Figure 3A and B). Local CaM activation was thus found to relate inversely to the diffusion coefficient of CaM (Figure 3C). These results suggest that CaM must diffuse at a moderate rate, as has been observed *in vivo,* to be activated and controlled in the local area. Moreover, these results imply that the cytoskeleton may regulate local signal transduction by influencing molecular diffusion in the area.

A local CaM diffusion system as a dual decoder

The dependence of Ca²⁺ signaling dynamics on frequency and current shapes of Ca²⁺ influxes was examined. First, three kinds of Ca²⁺ bursting influxes were applied to the model spine (Figure 4A). To see solely the effect of frequency here, each burst contained the same number of Ca²⁺ influxes and hence the same quantity of Ca²⁺ ions. As shown in Figure 2A and B, there was no cumulative effect in local Ca²⁺ (Figure 4C), whereas both global Ca²⁺ and local active CaM accumulated depending on the frequency (Figure 4B and D). Next, the shape of Ca²⁺ influxes is another important characteristic because it is known that current shape depends on the two main subtypes of NMDARs, NR2A- and NR2B-containing NMDA receptors; the current produced by NR2A-containing NMDARs has a higher amplitude and a shorter duration than that produced by NR2B-containing receptors (Erreger *et al*, 2005). To investigate the effect of current shape on Ca²⁺ signaling, we prepared three current shapes including the same quantity of Ca²⁺ (Figure 4E). Different current shapes induced different peak values of Ca²⁺ concentration (Figure 4G) and CaM activation (Figure 4H) in the local area, but the difference was not very prominent for global Ca²⁺ (Figure 4F).

In the induction of synaptic plasticity, the direction and strength depend on the frequency of Ca²⁺ influxes (Dudek and Bear, 1992; Markram *et al*, 1997; Johnston *et al*, 2003) and NMDAR subtypes (Liu *et al*, 2004a; Massey *et al*, 2004). This frequency-dependent and receptor-specific regulation is evidence that Ca²⁺ signaling simultaneously transfers both the frequency and influx rate signals to downstream cascades ('dual decoder') in levels of Ca²⁺, CaM, or CaM effectors. We propose that such a dual regulation can be explained by
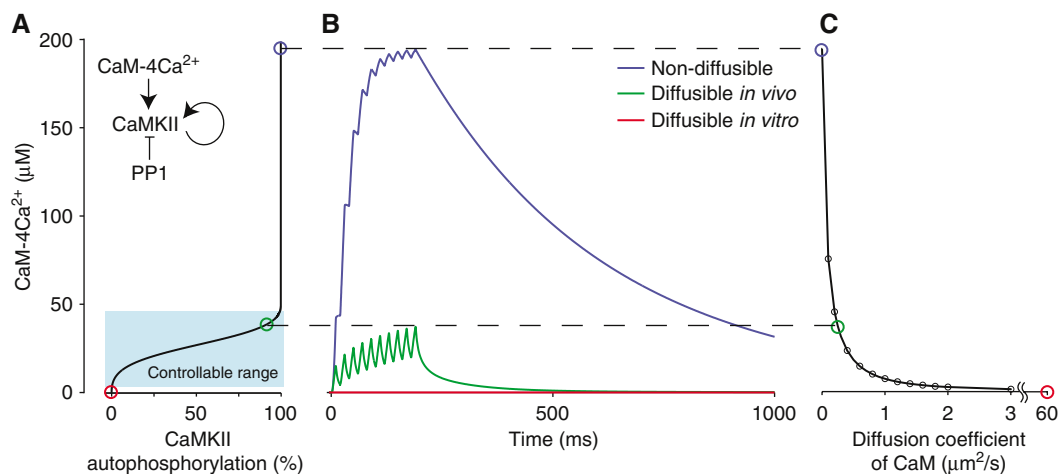

Figure 3 The dependence of local CaM activation on CaM diffusion. (**A**) Estimated autophosphorylation percent of CaMKII responding to the concentration of CaM-4Ca²⁺ in the condition where the endogenous factor PP1 dephosphorylates CaMKII (Winder and Sweatt, 2001). Using experimentally measured parameters in the Hill's equation for the autophosphorylation of CaMKII against Ca²⁺ *in vitro* (Bradshaw *et al*, 2003), we depicted the relationship of CaMKII activity with CaM-4Ca²⁺ to indicate a rough criterion for how much CaM activity is required for transducing signals to CaM effector proteins. The estimation method is detailed in Supplementary Figure 3. The approximate concentration range in which active CaM (CaM-4Ca²⁺) can control CaMKII autophosphorylation (0–100%) is depicted in light blue color. Note that this outcome is not very sensitive to the affinity change of CaM for Ca²⁺ (see Supplementary Figure 3). (**B**) The time course of CaM-4Ca²⁺ formation in the local area (25–50 nm away from the NMDARs). The diffusion coefficients of CaM were 0 (blue), 60 (red), and 0.25 μm²/s (green), representing nondiffusible CaM, diffusible CaM as estimated *in vitro* (Yang *et al*, 2001), and diffusible CaM as measured *in vivo* (Luby-Phelps *et al*, 1995), respectively. Ca²⁺ inputs were the same as in Figure 1B. (**C**) The dependence of the peak concentration of local CaM-4Ca²⁺ on the diffusion coefficients of CaM.
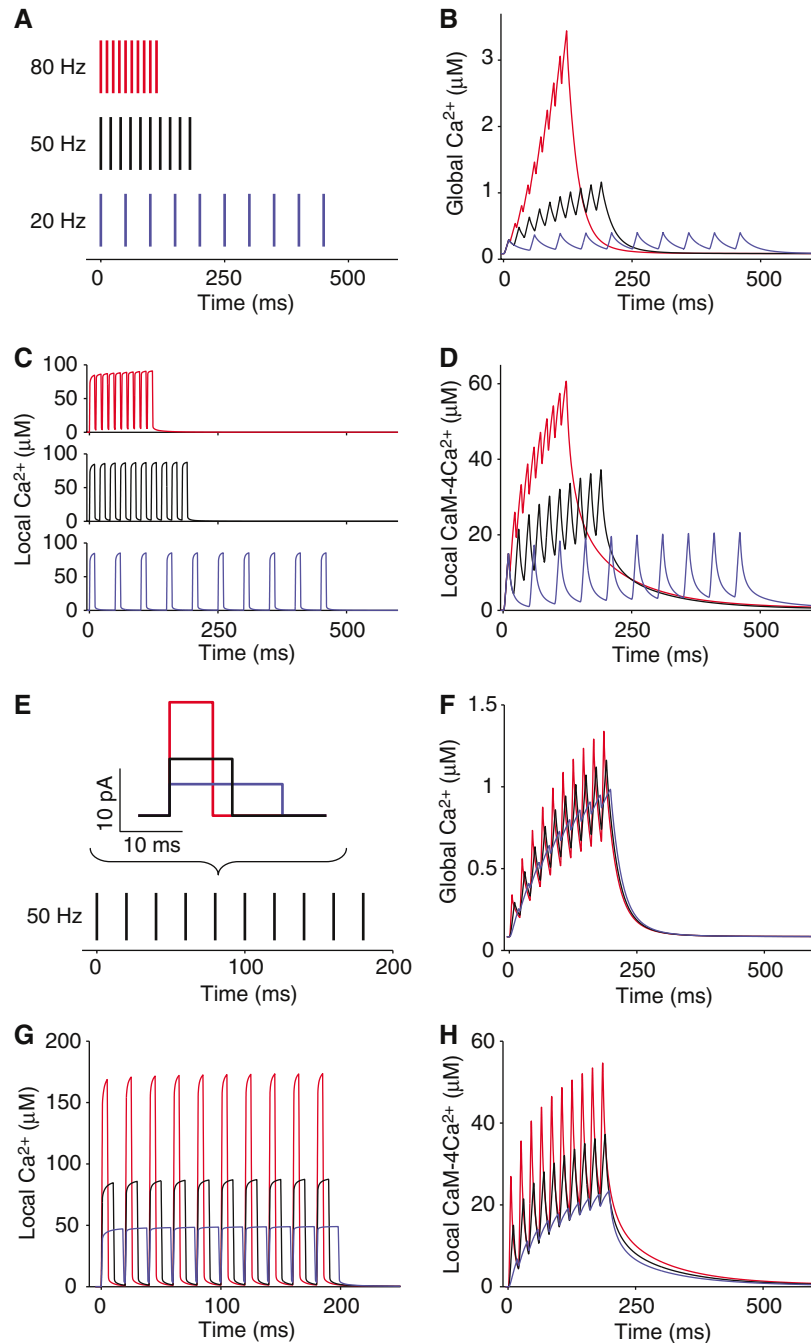
Figure 4 The time course of Ca^{2+} signaling in response to various frequencies and current shapes of Ca^{2+} influxes. (**A**) Three frequency patterns of Ca^{2+} influxes. Each injected current was the same as shown in Figure 1B. (**B–D**) The responses of global Ca^{2+} (B), local Ca^{2+} (C), and local CaM (D) to the three frequencies of Ca^{2+} influxes: blue: 20 Hz; black: 50 Hz; and red: 80 Hz. (**E**) Three current shapes of Ca^{2+} influx, which was applied at a fixed frequency of 50 Hz. The total quantity of Ca^{2+} ions in each current was set constant. (**F–H**) The responses of global Ca^{2+} (F), local Ca^{2+} (G), and local CaM (H) to the Ca^{2+} influxes, which each contains one of three different current shapes: blue: wide; black: medium; and red: narrow.

integrating the results of Figure 4. To examine if responses of Ca^{2+} and CaM in local and global area correlated with the frequency and influx rate signals, peak responses of Ca^{2+} signaling to these two input features are summarized in Figure 5. Here, for simple representation of the influx rate, the shape of a rectangular current was characterized by the amplitude and time width for a fixed total quantity of Ca^{2+} ions.

The Ca^{2+} level in the global area depended on the frequency of Ca^{2+} influxes, but not significantly on the influx rate (Figure 5A and C, left panels), suggesting that the dual decoder does not work in global Ca^{2+} signaling. In contrast, the local Ca^{2+} level was proportional to the influx rate but independent of the frequency (Figure 5A and C, right panels). For local CaM activation, the frequency of the influxes and the influx rate were directly proportional to the amount of activated CaM
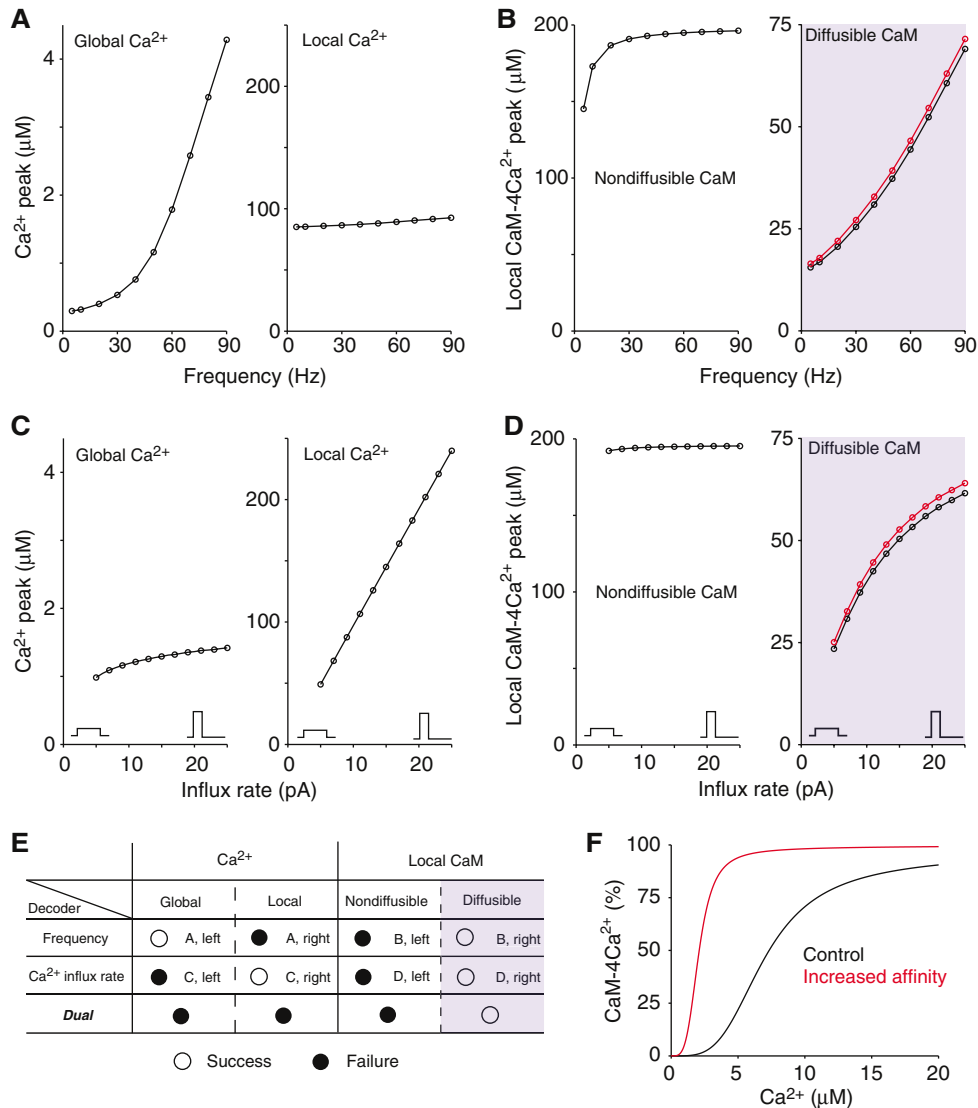
Figure 5 The ability of Ca^{2+} and CaM to decode the frequency and the influx rate of Ca^{2+} influxes. (**A, B**) Decoding by Ca^{2+} (A) and CaM (B) of the frequency of Ca^{2+} influxes. (**C, D**) Decoding by Ca^{2+} (C) and CaM (D) of the influx rate of the Ca^{2+} influxes. The horizontal axis denotes the amplitude of the rectangular current. The influx rate is characterized as the current amplitude. The duration of the current varied inversely with the amplitude of the current to keep the total quantity of Ca^{2+} ions. (A, C) Peak plots of the Ca^{2+} concentration in the local area (left panel) and in the global area (> 350 nm from the NMDARs) (right panel). (B, D) Peak plots of the CaM-4Ca^{2+} concentration in the local area for the nondiffusible CaM model (left panel) and the diffusible CaM model using the CaM diffusion coefficient observed *in vivo* (Luby-Phelps *et al*, 1995) (right panel). Red lines indicate the cases in which the affinity dependence of CaM for Ca^{2+} on CaM effector proteins was considered, as shown in (F). (**E**) A summary of the decoding abilities of Ca^{2+} and CaM. If the peak response correlated linearly with the frequency or the influx rate, decoding is regarded as success (an open circle), otherwise, as failure (a filled circle). Correspondence to subfigures is also shown; for example, 'A, left' means this decoding success can be observed in the left panel of subfigure (A). (**F**) Dose–response curve of CaM for Ca^{2+}. This curve is derived from kinetic parameters of CaM using CaM4Ca$=$CaM$_{total}$ $K_1 K_2 K_3 K_4$ Ca^4/$(1 + K_1$ Ca$^1 + K_1 K_2$ Ca$^2 + K_1 K_2 K_3$ Ca$^3 + K_1 K_2 K_3 K_4$ Ca^4), $K_i = K_{f_i}/K_{b_i}$ ($i=1$–4). Black and red lines indicate the cases without and with the kinetic parameter values of backward reaction in the third and fourth binding of Ca^{2+} being one-tenth; the red-colored condition represents the increase in the affinity of CaM for Ca^{2+} due to the interaction with CaM effector proteins.

(CaM-4Ca^{2+}) when the CaM diffusion coefficient measured *in vivo* was used (Figure 5B and D, right panels), but not when CaM was prevented from diffusing (Figure 5B and D, left panels) (the time course of nondiffusible CaM activity is shown in Supplementary Figure 13). Thus, this local CaM diffusion system is necessary for Ca^{2+} signaling to be able to dual-decode the frequency of influxes and the shape of currents (Figure 5E). In particular, the ability to detect the influx rate (current shape) may be the basis of receptor-specific regulation of synaptic signal transduction.

One or two Ca^{2+}-bound CaM molecules interact with CaM effector proteins such as CaMKII and adenylate cyclase, and the interactions increase the affinity of CaM for Ca^{2+} by reducing the dissociating reaction rate rather than by increasing the binding reaction rate (Johnson *et al*, 1996). When we introduced an increased affinity, by employing a one-tenth value for the kinetic parameter, to the backward reaction in the third and fourth binding of Ca^{2+} (Figure 5F), little effect was found on the local CaM activity (red lines in Figure 5B and D, right panels), whereas global CaM activation was facilitated as
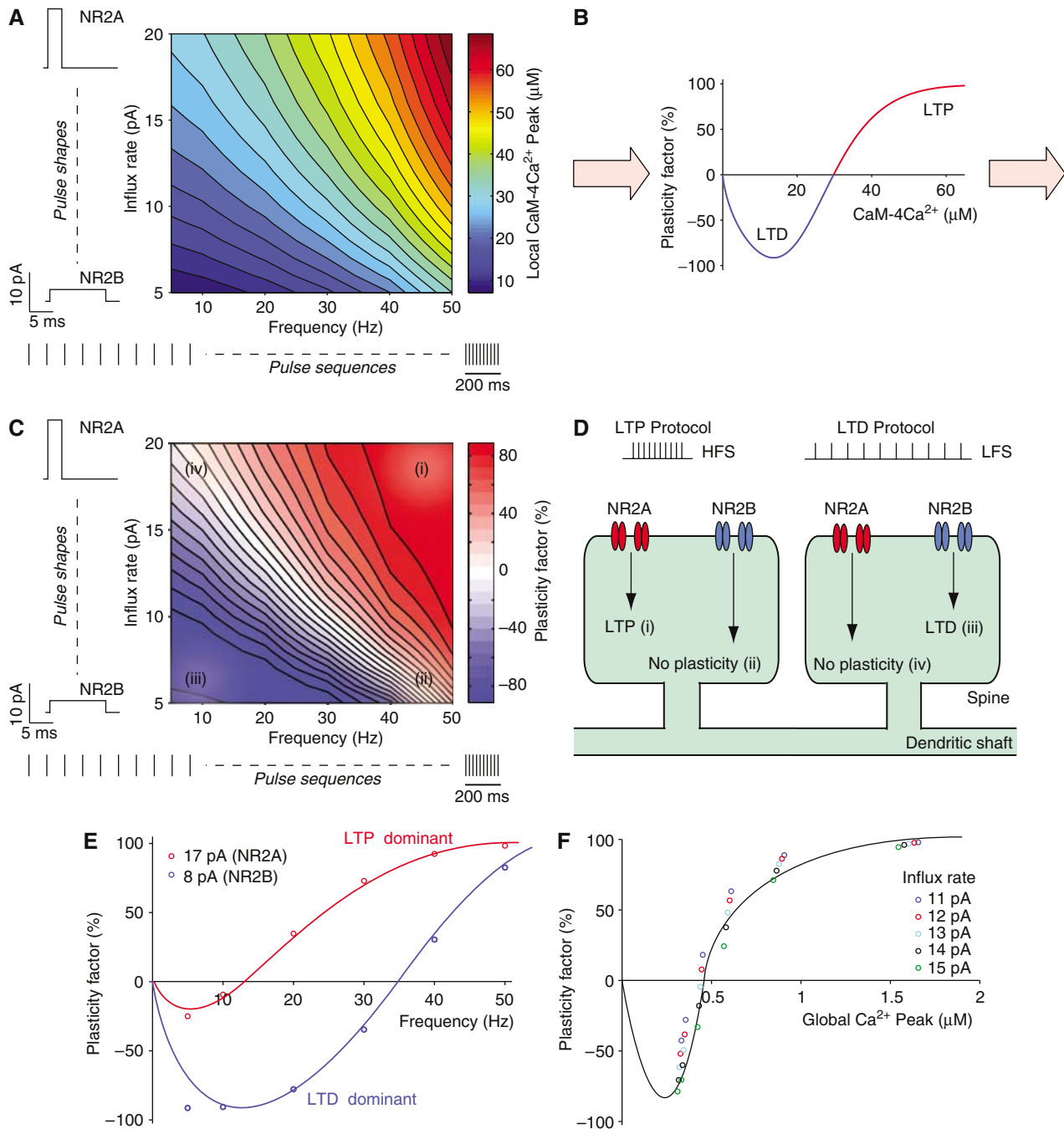
Figure 6 Reproduction of frequency- and NMDAR subtype-based regulation of synaptic plasticity. (**A**) The peak concentrations of CaM-4Ca^{2+} in the local area, computed after 100 identical Ca^{2+} influxes were applied to the model spine, are displayed. The frequency (horizontal axis) and the influx rate (vertical axis) of the Ca^{2+} influxes were varied in each trial. (**B**) Synaptic plasticity was modeled by a U-shaped function of the CaM-4Ca^{2+} concentration. The plasticity factor is expressed as positive and negative values for LTP and LTD, respectively. The boundary between LTD and LTP was set at 30 μM CaM-4Ca^{2+}, which corresponds to the concentration necessary for around 65% CaMKII activity at equilibrium (see Figure 3A). (**C**) The resultant synaptic plasticity computed from the peak CaM-4Ca^{2+} concentration (A) using the U-shaped function (B). The meaning of labels (i–iv) is explained in the text. (**D**) An illustration of the regulation of synaptic plasticity by the subtypes of NMDARs. The labels (i–iv) correspond to those in (C). (**E**) The dependence of synaptic plasticity on the frequency of Ca^{2+} influxes for two influx rate values, corresponding to NR2A- and NR2B-containing receptors. These data are extracted from (C). The blue and red curves are schematic, each roughly interpolating the circles. (**F**) The relationship between synaptic plasticity and the global Ca^{2+} level in the model spine. The horizontal and vertical axes denote the peak of global Ca^{2+} concentration and the plasticity factor, respectively. These data are also extracted from (C), with a variety of frequencies (5, 10, 20, 30, 40, and 50 Hz) and influx rates (11–15 pA). As in (E), the black curve shows schematic interpolation. Note that the plasticity factor is obtained by applying the U-shaped function (B) to the local CaM-4Ca^{2+} concentration (A), not to the global Ca^{2+} concentration.

expected (Supplementary Figure 14). This result implies that dual decoding is not influenced by CaM affinity. Moreover, the dual decoding was found to be robust against variations in the buffering, excretion system, spine morphology, and current shapes of injected Ca^{2+} influxes (see Supplementary Figures 15–19).

Synaptic plasticity induced by local CaM activity

The dependence of CaM activation on the frequency and current shapes of Ca^{2+} influxes is comprehensively evaluated in Figure 6A. For the bridge between CaM activation (Figure 6A) and the expression of LTP and LTD (represented by the plasticity factor), we assumed that the plasticity factor is defined by a U-shaped function of the CaM-4Ca^{2+} concentration (Figure 6B).

The U-shaped function was mathematically derived from the network structure of downstream cascade (CaMKII/calcineurin-PP1 system) (D'Alcantara *et al*, 2003), based on the idea that the change in synaptic weight regulated by phosphorylation of AMPA receptors is determined by a balance between kinase (CaMKII) and phosphatase (calcineurin, PP1) activities (Lisman, 1989). In great deals of signaling cascades involving the regulation of synaptic plasticity, CaM behaves as a hub and is believed to integrate Ca^{2+} signals (Xia and Storm, 2005). Then, it is reasonable to evaluate synaptic plasticity outcomes with respect to CaM activity.

Applying this U-shaped function to the calculated levels of activated CaM obtained from burst stimulations with variable frequencies and influx rates resulted in two-dimensional synaptic plasticity as shown in Figure 6C. The parameter space can be divided into four regions: (i) the stimulations induced LTP, (iii) the stimulations induced LTD, and (ii) and (iv) no plasticity was induced.

We propose here that our model can explain the NMDAR subtype-specific regulation of synaptic plasticity (Liu *et al*, 2004a; Massey *et al*, 2004) (Figure 6C and D). Under control conditions, high-frequency stimulation (HFS) causes both subtypes of NMDARs to respond in this spine, leading to plasticity factor values in regions (i) and (ii), whose combination results in LTP. If the NR2A subtypes are blocked, only region (ii) remains and no plasticity is induced. If the NR2B subtypes are blocked, only region (i) remains and LTP is induced. On the other hand, low-frequency stimulation (LFS) results in plasticity factor values in regions (iii) and (iv) thereby inducing LTD. If the NR2B subtypes are blocked, region (iii) disappears and no plasticity is generated. Conversely, if the NR2A subtypes are blocked, only region (iv) disappears and LTD is induced.

In addition, our model reproduced the dependence of synaptic plasticity on the frequency of synaptic inputs being U-shaped (Figure 6C) (Dudek and Bear, 1992; Johnston *et al*, 2003). Furthermore, consistent with the observation that during neuronal development, the NR2A/NR2B ratio in NMDARs increases (Liu *et al*, 2004b) and LTP gradually becomes dominant over LTD (Puyal *et al*, 2003), we found that LTP became dominant when a high influx rate was applied to the model (Figure 6E). We also found a U-shaped relationship between the global Ca^{2+} concentration and synaptic plasticity

(Figure 6F). This reminds us of the conventionally discussed relationship between plasticity and the spatially averaged Ca^{2+} level, which has been observed in Ca^{2+} imaging studies (Hansel *et al*, 1997; Cormier *et al*, 2001; Johnston *et al*, 2003). It should be noted here that the plasticity factor in our model was determined by local CaM activity and not by global Ca^{2+} levels (Figure 6B).

Discussion

The connections between spatial factors in signal transduction and specific biological functions have not been sufficiently investigated. We have shown the significance of spatial factors, such as local reactions within the Ca^{2+} nano-domain and the diffusion of Ca^{2+} effector proteins, to the Ca^{2+} signaling required for synaptic plasticity.

Ca^{2+} nano-domain ($>90\,\mu M$, $<50\,nm$) appeared during the application of Ca^{2+} influxes (Figure 1B). This high Ca^{2+} concentration activated CaM excessively because of inherent strong affinity of CaM for Ca^{2+} when CaM could not diffuse (Figure 3B). Such excessive CaM activation was, however, prevented by diffusion of CaM itself, as shown in Figure 3B and C. As long as CaM diffuses at a moderate rate as *in vivo*, local CaM activity remains in an appropriate range, which is useful to control downstream signaling (Figure 3A). This 'local CaM diffusion system' functions as a 'dual decoder' of both the frequency of Ca^{2+} influxes and the current shapes generated by two distinct NMDA receptor subtypes (Erreger *et al*, 2005) (Figure 5B and D, right panels). Frequency decoding is realized by CaM diffusion transferring transient frequency-independent Ca^{2+} responses into accumulated responses of CaM, whereas influx rate decoding is realized by means of Ca^{2+} levels before the signals are transduced into the CaM activity. The dual decoding in local Ca^{2+} signaling is strongly robust, regardless of how global Ca^{2+} behaves.

Previous studies proposed that CaMKII detects the stimulation frequency by becoming autophosphorylated, thereby translating the frequency level into the strength of LTP. CaMKII was observed to act as a frequency decoder of Ca^{2+} stimulation *in vitro* and *in vivo* (De Koninck and Schulman, 1998; Eshete and Fields, 2001). On the other hand, a biochemical study revealed that the phosphorylation state of CaMKII at equilibrium depends on the Ca^{2+} concentration (Bradshaw *et al*, 2003), hence on CaM activity (Figure 3A). In our simulation, the phosphorylation level of CaMKII was in effective determined by the peak concentration of active CaM, because the local concentration of active CaM was rapidly increased and saturated as Ca^{2+} stimulation and the saturated level depended on the frequency and the influx rate of Ca^{2+} stimulation. This is the reason why we evaluated the decoder's ability in relation to the peak response of active CaM, but not to its temporal integration. Therefore, our results indicate that the local CaM diffusion system, rather than CaMKII, plays the main role in decoding the information of synaptic stimulation (Figure 5).

The dual decoding by the local CaM diffusion system provides a mechanism for both the frequency-dependent and NMDAR subtype-specific regulation of synaptic plasticity (Figure 6C); our model of local Ca^{2+} signaling with

constrained molecular diffusion successfully realized the receptor-specific regulation, which could not be accomplished by global Ca^{2+} signaling. Moreover, our model reproduced the observed developmental shift from LTD to LTP (Figure 6E).

We also found that the relationship between the global Ca^{2+} concentration and the synaptic plasticity induced by local CaM activity was U-shaped (Figure 6F). Currently, it is thought that synaptic plasticity is simply determined by the Ca^{2+} concentration in a U-shaped fashion (Hansel *et al*, 1997; Yang *et al*, 1999; Cormier *et al*, 2001; Johnston *et al*, 2003); high and moderate Ca^{2+} concentrations induce LTP and LTD, respectively. In this simplified scheme, however, the Ca^{2+} concentration is averaged over the entire spine, and hence does not reflect local Ca^{2+} signaling. On the other hand, recent experimental studies showed that local Ca^{2+} signaling around Ca^{2+} channels regulates the induction of LTP (Hoffman *et al*, 2002; Yasuda *et al*, 2003), suggesting that synaptic plasticity cannot be explained simply by the averaged Ca^{2+} concentration, and that local Ca^{2+} signaling must be taken into account. We, therefore, speculate that the conventional 'global Ca^{2+} hypothesis' is too macroscopic to allow us to understand the complicated regulation scheme of synaptic plasticity.

Local CaM activation was found to be strongly affected by the diffusion coefficient of CaM itself (Figure 3C). CaM diffusion may be regulated by cytoskeletal structures such as actin filaments. The polymerization of actin is affected by synaptic stimulation; HFS facilitates actin polymerization, whereas LFS facilitates actin depolymerization (Okamoto *et al*, 2004), suggesting that HFS or LFS would suppress or facilitate CaM diffusion, respectively. These observations suggest that synaptic plasticity also depends on the temporal change in the CaM diffusion coefficient caused by previous synaptic stimulations. When an LFS occurs, the induced actin depolymerization facilitates CaM diffusion, making it more difficult to activate CaM and induce LTP. After an HFS, in contrast, it becomes easier to induce LTP. These predictions are consistent with 'meta-plasticity', an observed experimental phenomenon in which the LTP resulting from an HFS was decreased if the stimulation followed a previously applied LFS that did not induce LTD (Fujii *et al*, 1991; O'Dell and Kandel, 1994; Mockett *et al*, 2002).

Although local Ca^{2+} dynamics have been investigated in other computational studies (Holmes and Levy, 1990; Zador *et al*, 1990; Naraghi and Neher, 1997; Markram *et al*, 1998; Tang *et al*, 2000; Franks *et al*, 2001), those studies did not discuss local CaM activation involving own diffusion and its responses to various characteristics of Ca^{2+} stimulations. A couple of studies modeled spatial Ca^{2+} signaling associated with LTP by introducing cylindrical morphology to a spine head (Holmes and Levy, 1990; Zador *et al*, 1990). This cylindrical approximation assumed that diffusion occurs only in the direction perpendicular to the membrane but not in the direction parallel to the membrane, which makes the discussion on the locality of Ca^{2+} signaling difficult. Another computational study has exhibited the frequency dependence of CaM response in an entire spine, which originates from the frequency dependence of global Ca^{2+} (Franks *et al*, 2001). However, local CaM activation and the diffusion process of CaM were not addressed in that study. Our spatial model

showed consistently that the global Ca^{2+} response is frequency-dependent (Figure 5A, left panel).

Ca^{2+} micro-domains ($< 1\,\mu m$) were directly identified in GABAergic interneurons even in the absence of special structures such as dendritic spines (Goldberg *et al*, 2003). In our study, we also showed the existence of a Ca^{2+} nano-domain ($< 50\,nm$), whose scale is comparable to that of PSD and much less than that of a dendritic spine (Figure 1B). Although these two kinds of local Ca^{2+} compartmentalizations have different scales, they may share a common molecular mechanism actualized by Ca^{2+} influx, buffering, and fast Ca^{2+} extrusion.

The issue of stochasticity of signal transduction in a dendritic spine is important because the number of signaling molecules in such a small region is often small. Stochastic properties of signal transduction pathways with positive-feedback loops, such as CaMKII autophosphorylation, are quite different from deterministic processes at the level of single spines (Hayer and Bhalla, 2005; Miller *et al*, 2005). However, experimental measurements of synaptic plasticity (i.e., EPSP) are spatial averages over a large number of synapses, and, moreover, they should be averaged temporally (i.e., trial average) when the direction or strength of plasticity is evaluated. Therefore, we expect that deterministic simulation is valid for assessing the spatiotemporally averaged response of a local CaM diffusion system, which does not involve a positive-feedback loop.

Ca^{2+} ions act as secondary messengers to transmit extracellular signals to intracellular proteins during a variety of cellular functions. The properties of local reactions (the biochemical processes) and molecular diffusion (the physical processes) can be extended to other molecular systems, such as axon guidance by growth cones controlled by Ca^{2+} signaling (Nishiyama *et al*, 2003), to gain an overall understanding of the subcellular biology.

Materials and methods

Geometry of model spine and diffusion processes

For simulating radial diffusion, the model spine ($1\,\mu m^3$) was divided into 15 elements of hemispherical shells with a thickness of 25 nm (from the 1st to the 14th shells) or 781.6 nm (the 15th shell) (Figure 1A and Supplementary Figure 1). Molecular diffusion from one shell to adjacent shells was introduced according to the difference between the concentrations in the shells:

$$\left(\frac{d[X]_n}{dt}\right)_{diffusion} = D_X \frac{A_{n-1,n}}{d_{n-1,n}V_n}([X]_{n-1} - [X]_n) + D_X \frac{A_{n,n+1}}{d_{n,n+1}V_n}$$
$$\times ([X]_{n+1} - [X]_n) \tag{1}$$

where $[X]_n$ denotes the concentration of diffusible molecules (Ca^{2+}, CaM, and mobile calcium-binding protein (CBP)) in the nth shell, D_X is the diffusion coefficient, $A_{n-1,n}$ is the surface area between the $(n-1)$th and the nth shells, $d_{n-1,n}$ is the distance between the shells' midpoints, and V_n is the volume of the nth shell. Molecular concentrations in each shell were assumed to be uniform. Diffusion of Ca^{2+} between a spine and a dendritic shaft was not considered, because spines are thought to be isolated compartments of signaling (Svoboda *et al*, 1996; Helmchen, 2002; Sabatini *et al*, 2002). We also confirmed that the diffusive exchange between the spine and the dendritic shaft does not significantly affect Ca^{2+} signaling in a spine (Supplementary Figure 20).

In this study, we used hemispherical approximation for spine head to simulate local Ca^{2+} signaling, in contrast to conventional

cylindrical approximation (Holmes and Levy, 1990; Zador *et al*, 1990). Compared with the cylindrical approximation, our model pays more attention to locality of Ca^{2+} signaling around a localized cluster of NMDARs: NR2A-containing NMDA receptors are localized specifically in synaptic clefts, whereas those containing NR2B tend to be localized far from the release sites of presynaptic vesicles (Collingridge *et al*, 2004; Liu *et al*, 2004b).

Ca^{2+} regulation

Ca^{2+} ions were injected through a number of NMDARs as a point source located at the center of the first shell (Figure 1A and Supplementary Figure 1). Ca^{2+} influx was given as a rectangular shape (Figure 1B, upper panel) and the concentration change was defined by

$$\left(\frac{\mathrm{d}[\mathrm{Ca}^{2+}]_{n=1}}{\mathrm{d}t}\right)_{\mathrm{influx}} = -\gamma I/(2FV_{n=1}) \qquad (2)$$

where γ denotes the fraction of current I carried by Ca^{2+} through the NMDARs and F is the Faraday's constant. Because the estimated number of NMDARs opened in a single spine by a synaptic spike is three (Nimchinsky *et al*, 2004) and the current through a single channel was measured at 3 pA (Pina-Crespo and Gibb, 2002), I was set at 9 pA (10 ms), except when examining the effect of Ca^{2+} influx rate on local Ca^{2+} signaling (Figures 4–6).

Extrusion of Ca^{2+} from the spine was modeled by three types of Ca^{2+} pumps (SERCA, Na$^+$/Ca^{2+} exchanger, and PMCA) situated only at the outermost (15th) shell (Figure 1A and Supplementary Figure 1). The Ca^{2+} extrusion process was described by Hill's equation:

$$\left(\frac{\mathrm{d}[\mathrm{Ca}^{2+}]_{n=15}}{\mathrm{d}t}\right)_{\mathrm{pump}} = -v_{\mathrm{max}}\frac{[\mathrm{Ca}^{2+}]_{n=15}^{h}}{[\mathrm{Ca}^{2+}]_{n=15}^{h} + K_{\mathrm{m}}^{h}} \qquad (3)$$

where v_{max} is the maximal velocity of Ca^{2+} clearance, K_{m} is the half-maximal concentration of Ca^{2+} for each pump, and h is the Hill coefficient. Leak Ca^{2+} flow was also added into the outermost shell with the leak constants $L_{\mathrm{extracell}}$ and L_{ER} (Figure 1A and Supplementary Figure 1):

$$\left(\frac{\mathrm{d}[\mathrm{Ca}^{2+}]_{n=15}}{\mathrm{d}t}\right)_{\mathrm{leak}} = -L_{\mathrm{extracell}}([\mathrm{Ca}^{2+}]_{n=15} - [\mathrm{Ca}^{2+}]_{\mathrm{extracell}})$$
$$- L_{\mathrm{ER}}([\mathrm{Ca}^{2+}]_{n=15} - [\mathrm{Ca}^{2+}]_{\mathrm{ER}}) \qquad (4)$$

where $[\mathrm{Ca}^{2+}]_{\mathrm{extracell}}$ and $[\mathrm{Ca}^{2+}]_{\mathrm{ER}}$ are Ca^{2+} concentrations outside the model spine and in the endoplasmic reticulum, respectively.

For Ca^{2+} buffering, we distributed five kinds of Ca^{2+}-binding proteins uniformly into the model spine: four kinds of immobile, and one mobile, CBPs. The kinetic parameters of immobile CBPs (fast CBP, medium CBP, slow CBP, and very-slow CBP) followed the previous models (Markram *et al*, 1998; Franks *et al*, 2001). Mobile CBPs, which are likely to contribute to Ca^{2+} dynamics, are diffusible and their diffusion coefficients are independent of Ca^{2+} binding in the model. Binding of Ca^{2+} ions to CBPs was modeled by the association and dissociation reactions:

$$\left(\frac{\mathrm{d}[\mathrm{Ca}^{2+}]_{n}}{\mathrm{d}t}\right)_{\mathrm{CBP}} = -k_{\mathrm{f}}[\mathrm{Ca}^{2+}]_{n}[\mathrm{CBP}]_{n} + k_{\mathrm{b}}[\mathrm{CBP}\cdot\mathrm{Ca}^{2+}]_{n} \qquad (5)$$

where k_{f} and k_{b} are the association and dissociation rates, respectively.

Calmodulin regulation

CaM has four binding sites for Ca^{2+} ions (two sites in each of the C- and N-terminal domains) and its transducer function was assumed to emerge when all four sites are occupied (CaM-4Ca^{2+}). Each Ca^{2+} binding step in this fourth-order reaction was calculated by

$$\left(\frac{\mathrm{d}[\mathrm{CaM}\cdot z\mathrm{Ca}^{2+}]_{n}}{\mathrm{d}t}\right)_{\mathrm{CaM}} = k_{\mathrm{f},z}[\mathrm{Ca}^{2+}]_{n}[\mathrm{CaM}\cdot(z-1)\mathrm{Ca}^{2+}]_{n}$$
$$- (k_{\mathrm{b},z} + k_{\mathrm{f},z+1})[\mathrm{CaM}\cdot z\mathrm{Ca}^{2+}]_{n}$$
$$+ k_{\mathrm{b},z+1}[\mathrm{CaM}\cdot(z+1)\mathrm{Ca}^{2+}]_{n} \qquad (6)$$

where $[\mathrm{CaM}\cdot z\mathrm{Ca}^{2+}]_{n}$ denotes the concentration of CaM bound by $z\mathrm{Ca}^{2+}$ ions, and $k_{\mathrm{f},z}$ and $k_{\mathrm{b},z}$ are the association and dissociation rates in the zth step reaction ($z=0, 1, 2, 3, 4$). Note that the association rate of N-terminal domains used in the model was one-tenth that measured *in vitro* (Luby-Phelps *et al*, 1995), because Ca^{2+} binding is interfered owing to the interaction of CaM with Mg^{2+} and K$^+$ ions, and the effective rates then decrease (Linse *et al*, 1991; Malmendal *et al*, 1999). The concentration of CaM was set at 200 µM in the model spine. For the diffusion coefficient of CaM, we used the value previously measured in smooth muscle cells (Luby-Phelps *et al*, 1995), except when examining model behaviors against various values of the diffusion coefficient (Figure 3C). The diffusion coefficient of CaM was assumed to be independent of Ca^{2+} binding.

In this biochemical model, we did not distinguish the kinetic parameters of Ca^{2+} binding with CaM free or trapped by CaM effector proteins. The rate constants were adopted from an *in vitro* experimental report; to use these experimentally measured values, which should be a mixture of the rate constants of free and trapped CaM, implicitly incorporates the effect of interaction between CaM and CaM effector proteins (Johnson *et al*, 1996). Furthermore, in the diffusion process, we did not model differential diffusions between free CaM and trapped CaM, and we adopted the diffusion coefficient measured *in vivo* (Luby-Phelps *et al*, 1995); this experimental value should also include the effect of interaction between CaM and CaM effector proteins. Therefore, recruitment of the reaction rate constants and diffusion coefficient measured *in vivo* represents the average dynamics of signaling mediated by free CaM and trapped CaM.

All parameters used in the control condition of our model are listed with their values in Supplementary Table 1. Simulations were performed using MATLAB (The Mathworks Inc., MA).

Supplementary information

Supplementary information is available at the *Molecular Systems Biology* website (www.nature.com/msb).

References

Augustine GJ, Santamaria F, Tanaka K (2003) Local calcium signaling in neurons. *Neuron* **40:** 331–346

Bhalla US (2002a) Biochemical signaling networks decode temporal patterns of synaptic input. *J Comput Neurosci* **13:** 49–62

Bhalla US (2002b) Mechanisms for temporal tuning and filtering by postsynaptic signaling pathways. *Biophys J* **83:** 740–752

Blackstone C, Sheng M (2002) Postsynaptic calcium signaling microdomains in neurons. *Front Biosci* **7:** d872–d885

Bliss T, Schoepfer R (2004) Neuroscience. Controlling the ups and downs of synaptic strength. *Science* **304:** 973–974

Bradshaw JM, Kubota Y, Meyer T, Schulman H (2003) An ultrasensitive Ca^{2+}/calmodulin-dependent protein kinase II-protein phosphatase 1 switch facilitates specificity in postsynaptic calcium signaling. *Proc Natl Acad Sci USA* **100:** 10512–10517

Collingridge GL, Isaac JT, Wang YT (2004) Receptor trafficking and synaptic plasticity. *Nat Rev Neurosci* **5:** 952–962

Cormier RJ, Greenwood AC, Connor JA (2001) Bidirectional synaptic plasticity correlated with the magnitude of dendritic calcium transients above a threshold. *J Neurophysiol* **85:** 399–406

D'Alcantara P, Schiffmann SN, Swillens S (2003) Bidirectional synaptic plasticity as a consequence of interdependent Ca^{2+}-controlled phosphorylation and dephosphorylation pathways. *Eur J Neurosci* **17:** 2521–2528

De Koninck P, Schulman H (1998) Sensitivity of CaM kinase II to the frequency of Ca^{2+} oscillations. *Science* **279:** 227–230

Dudek SM, Bear MF (1992) Homosynaptic long-term depression in area CA1 of hippocampus and effects of *N*-methyl-D-aspartate receptor blockade. *Proc Natl Acad Sci USA* **89:** 4363–4367

Erreger K, Dravid SM, Banke TG, Wyllie DJ, Traynelis SF (2005) Subunit-specific gating controls rat NR1/NR2A and NR1/NR2B NMDA channel kinetics and synaptic signaling profiles. *J Physiol* **563:** 345–358

Eshete F, Fields RD (2001) Spike frequency decoding and autonomous activation of Ca^{2+}-calmodulin-dependent protein kinase II in dorsal root ganglion neurons. *J Neurosci* **21:** 6694–6705

Franks KM, Bartol TM, Sejnowski TJ (2001) An MCell model of calcium dynamics and frequency-dependence of calmodulin activation in dendritic spines. *Neurocomputing* **38–40:** 9–16

Fujii S, Saito K, Miyakawa H, Ito K, Kato H (1991) Reversal of long-term potentiation (depotentiation) induced by tetanus stimulation of the input to CA1 neurons of guinea pig hippocampal slices. *Brain Res* **555:** 112–122

Goldberg JH, Tamas G, Aronov D, Yuste R (2003) Calcium microdomains in aspiny dendrites. *Neuron* **40:** 807–821

Hansel C, Artola A, Singer W (1997) Relation between dendritic Ca^{2+} levels and the polarity of synaptic long-term modifications in rat visual cortex neurons. *Eur J Neurosci* **9:** 2309–2322

Hayer A, Bhalla US (2005) Molecular switches at the synapse emerge from receptor and kinase traffic. *PLoS Comput Biol* **1:** e20

Helmchen F (2002) Raising the speed limit—fast Ca(2+) handling in dendritic spines. *Trends Neurosci* **25:** 438–441, discussion 441

Hoffman DA, Sprengel R, Sakmann B (2002) Molecular dissection of hippocampal theta-burst pairing potentiation. *Proc Natl Acad Sci USA* **99:** 7740–7745

Holmes WR, Levy WB (1990) Insights into associative long-term potentiation from computational models of NMDA receptor-mediated calcium influx and intracellular calcium concentration changes. *J Neurophysiol* **63:** 1148–1168

Holthoff K, Tsay D, Yuste R (2002) Calcium dynamics of spines depend on their dendritic location. *Neuron* **33:** 425–437

Johnston D, Christie BR, Frick A, Gray R, Hoffman DA, Schexnayder LK, Watanabe S, Yuan LL (2003) Active dendrites, potassium channels and synaptic plasticity. *Philos Trans R Soc London B* **358:** 667–674

Johnson JD, Snyder C, Walsh M, Flynn M (1996) Effects of myosin light chain kinase and peptides on Ca^{2+} exchange with the N- and C-terminal Ca^{2+} binding sites of calmodulin. *J Biol Chem* **271:** 761–767

Kennedy MB (2000) Signal-processing machines at the postsynaptic density. *Science* **290:** 750–754

Linse S, Helmersson A, Forsen S (1991) Calcium binding to calmodulin and its globular domains. *J Biol Chem* **266:** 8050–8054

Lisman J (1989) A mechanism for the Hebb and the anti-Hebb processes underlying learning and memory. *Proc Natl Acad Sci USA* **86:** 9574–9578

Lisman J, Schulman H, Cline H (2002) The molecular basis of CaMKII function in synaptic and behavioural memory. *Nat Rev Neurosci* **3:** 175–190

Liu L, Wong TP, Pozza MF, Lingenhoehl K, Wang Y, Sheng M, Auberson YP, Wang YT (2004a) Role of NMDA receptor subtypes in governing the direction of hippocampal synaptic plasticity. *Science* **304:** 1021–1024

Liu XB, Murray KD, Jones EG (2004b) Switching of NMDA receptor 2A and 2B subunits at thalamic and cortical synapses during early postnatal development. *J Neurosci* **24:** 8885–8895

Luby-Phelps K, Hori M, Phelps JM, Won D (1995) Ca(2+)-regulated dynamic compartmentalization of calmodulin in living smooth muscle cells. *J Biol Chem* **270:** 21532–21538

Malmendal A, Linse S, Evenas J, Forsen S, Drakenberg T (1999) Battle for the EF-hands: magnesium–calcium interference in calmodulin. *Biochemistry* **38:** 11844–11850

Markram H, Lubke J, Frotscher M, Sakmann B (1997) Regulation of synaptic efficacy by coincidence of postsynaptic APs and EPSPs. *Science* **275:** 213–215

Markram H, Roth A, Helmchen F (1998) Competitive calcium binding: implications for dendritic calcium signaling. *J Comput Neurosci* **5:** 331–348

Massey PV, Johnson BE, Moult PR, Auberson YP, Brown MW, Molnar E, Collingridge GL, Bashir ZI (2004) Differential roles of NR2A and NR2B-containing NMDA receptors in cortical long-term potentiation and long-term depression. *J Neurosci* **24:** 7821–7828

Matus A (2000) Actin-based plasticity in dendritic spines. *Science* **290:** 754–758

Miller P, Zhabotinsky AM, Lisman JE, Wang XJ (2005) The stability of a stochastic CaMKII switch: dependence on the number of enzyme molecules and protein turnover. *PLoS Biol* **3:** e107

Mockett B, Coussens C, Abraham WC (2002) NMDA receptor-mediated metaplasticity during the induction of long-term depression by low-frequency stimulation. *Eur J Neurosci* **15:** 1819–1826

Murthy VN, Sejnowski TJ, Stevens CF (2000) Dynamics of dendritic calcium transients evoked by quantal release at excitatory hippocampal synapses. *Proc Natl Acad Sci USA* **97:** 901–906

Nakada C, Ritchie K, Oba Y, Nakamura M, Hotta Y, Iino R, Kasai RS, Yamaguchi K, Fujiwara T, Kusumi A (2003) Accumulation of anchored proteins forms membrane diffusion barriers during neuronal polarization. *Nat Cell Biol* **5:** 626–632

Naraghi M, Neher E (1997) Linearized buffered Ca^{2+} diffusion in microdomains and its implications for calculation of [Ca^{2+}] at the mouth of a calcium channel. *J Neurosci* **17:** 6961–6973

Nimchinsky EA, Yasuda R, Oertner TG, Svoboda K (2004) The number of glutamate receptors opened by synaptic stimulation in single hippocampal spines. *J Neurosci* **24:** 2054–2064

Nishiyama M, Hoshino A, Tsai L, Henley JR, Goshima Y, Tessier-Lavigne M, Poo MM, Hong K (2003) Cyclic AMP/GMP-dependent modulation of Ca^{2+} channels sets the polarity of nerve growth-cone turning. *Nature* **423:** 990–995

O'Dell TJ, Kandel ER (1994) Low-frequency stimulation erases LTP through an NMDA receptor-mediated activation of protein phosphatases. *Learn Mem* **1:** 129–139

Okamoto K, Nagai T, Miyawaki A, Hayashi Y (2004) Rapid and persistent modulation of actin dynamics regulates postsynaptic reorganization underlying bidirectional plasticity. *Nat Neurosci* **7:** 1104–1112

Petersen JD, Chen X, Vinade L, Dosemeci A, Lisman JE, Reese TS (2003) Distribution of postsynaptic density (PSD)-95 and Ca^{2+}/calmodulin-dependent protein kinase II at the PSD. *J Neurosci* **23:** 11270–11278

Pina-Crespo JC, Gibb AJ (2002) Subtypes of NMDA receptors in new-born rat hippocampal granule cells. *J Physiol* **541:** 41–64

Popov S, Poo MM (1992) Diffusional transport of macromolecules in developing nerve processes. *J Neurosci* **12:** 77–85

Puyal J, Grassi S, Dieni C, Frondaroli A, Dememes D, Raymond J, Pettorossi VE (2003) Developmental shift from long-term depression to long-term potentiation in the rat medial vestibular nuclei: role of group I metabotropic glutamate receptors. *J Physiol* **553:** 427–443

Rusakov DA, Scimemi A, Walker MC, Kullmann DM (2004) Comment on 'Role of NMDA receptor subtypes in governing the direction of hippocampal synaptic plasticity'. *Science* **305:** 1912 author reply

Sabatini BL, Oertner TG, Svoboda K (2002) The life cycle of Ca(2+) ions in dendritic spines. *Neuron* **33:** 439–452

Sheng M, Lee SH (2000) Growth of the NMDA receptor industrial complex. *Nat Neurosci* **3:** 633–635

Svoboda K, Tank DW, Denk W (1996) Direct measurement of coupling between dendritic spines and shafts. *Science* **272:** 716–719

Tang Y, Schlumpberger T, Kim T, Lueker M, Zucker RS (2000) Effects of mobile buffers on facilitation: experimental and computational studies. *Biophys J* **78:** 2735–2751

Winder DG, Sweatt JD (2001) Roles of serine/threonine phosphatases in hippocampal synaptic plasticity. *Nat Rev Neurosci* **2:** 461–474

Wong TP, Liu L, Sheng M, Wang YT (2004) Response to comment on 'Role of NMDA receptor subtypes in governing the direction of hippocampal synaptic plasticity'. *Science* **305:** 1912

Xia Z, Storm DR (2005) The role of calmodulin as a signal integrator for synaptic plasticity. *Nat Rev Neurosci* **6:** 267–276

Yang C, Jas GS, Kuczera K (2001) Structure and dynamics of calcium-activated calmodulin in solution. *J Biomol Struct Dyn* **19:** 247–271

Yang SN, Tang YG, Zucker RS (1999) Selective induction of LTP and LTD by postsynaptic [Ca^{2+}]$_i$ elevation. *J Neurophysiol* **81:** 781–787

Yasuda R, Sabatini BL, Svoboda K (2003) Plasticity of calcium channels in dendritic spines. *Nat Neurosci* **6:** 948–955

Zador A, Koch C, Brown TH (1990) Biophysical model of a Hebbian synapse. *Proc Natl Acad Sci USA* **87:** 6718–6722